J Electroceram (2012) 28:89–94
DOI 10.1007/s10832-012-9684-9

Doping effects on dynamical physical properties of $Ca_{0.6}Sr_{0.4}Bi_4Ti_4O_{15}$ ferroelectric ceramics with layered-perovskite structure

M. S. Islam · J. Kano · Q. R. Yin · S. Kojima

Received: 4 January 2010 / Accepted: 16 January 2012 / Published online: 29 January 2012

Abstract The change of electrical and lattice dynamical properties of ferroelectric $Ca_{0.6}Sr_{0.4}Bi_4Ti_4O_{15}$ (CSBT) ceramics were studied by doping with 0.1 wt.% of CeO_2 and MnO_2. The loss tangent and the AC conductivity decreased markedly due to the reduction of charge carrier. The activation energy of doped-CSBT increased owing to the reduction of intrinsic defects in the crystal lattice. For doped and pure CSBT, the appearance of thermal hysteresis and the satisfaction of the Cure-Weiss law by the dielectric susceptibility data assigned the first order nature of a ferroelectric phase transition. Especially in ferroelectric phases, the soft optic phonon mode showed the significant softening towards T_1 (at T_1, the square of soft mode frequency $\omega_s^2 \rightarrow 0$) and ω_s^2 was approximately proportional to T_1-T, where T_1 is ~70°C above T_C=672°C, demonstrated a first order displacive nature of a ferroelectric phase transition. The invariance of lattice dynamical feature indicated that the crystal lattice did not influence markedly by the doping ions.

Keywords Layered-ferroelectrics · AC in conductivity · Phase transition · Soft mode

1 Introduction

Aurivillius bismuth layered-structure compounds (BLSFs) have attracted much attention for its high Curie temperature T_C, fatigue-free, and environmentally friendly nature, and become potential candidates for the application of electric and piezoelectric devices [1–4]. The chemical formula of this series is expressed as $Bi_2A_{m-1}B_mO_{3m+3}=(Bi_2O_2)^{2+}(A_{m-1}B_mO_{3m+1})^{2-}$; A is mono-, di- and trivalent ions or a mixture of them, B is tetra-, penta-, and hexavalent ions, the subscript m and m-1 are the numbers of oxygen octahedra and pseudo-perovskite units in the pseudo-perovskite layers, respectively. The crystal structure of BLSFs consists of pseudo-perovskite layers interleaved with the bismuth oxide $(Bi_2O_2)^{2+}$ layers along the c-axis [5–9]. The $CaBi_4Ti_4O_{15}$ (CBT) is one of the important member of BLSFs family for high temperature piezoelectric applications owing to its low electric conductivity, low dielectric loss, high T_C (790°C), and easy to fabrication by the conventional solid state reaction [10–13]. However, the relatively low piezoelectric response and large temperature dependence is the main obstacle for the commercialization [14]. The piezoelectric properties of CBT are largely enhanced by the partial replacement of the A-site calcium (Ca^{2+}) ion with the strontium (Sr^{2+}) ion, nevertheless T_C reduces owing to the large ionic radius (Ca=1.04 and Sr=1.20 Å). The Sr-doped CBT with the composition $Ca_{0.6}Sr_{0.4}Bi_4Ti_4O_{15}$ (CSBT) shows the best piezoelectric performance, and the observed piezoelectric coefficient and the dc resistively is decuply higher than the CBT and $SrBi_4Ti_4O_{15}$ (SBT) [11]. Therefore, CSBT is appeared as a potential candidate for high temperature applications. However, further modification is necessary for better ferroelectric and electrical performance.

Element doping is known to an effective route to improve piezoelectric and ferroelectric properties. In general, doping could be in oxide layers and/or in perovskite layers (A- or B-sites). Subbarro reported that the T_C of BLSFs decreases when the size of the A-site cations increase [15], while Forbess et al. found that the T_C increases and the electrical properties are improved markedly due to the replacement of

M. S. Islam (✉) · J. Kano · S. Kojima
Graduate School of Pure and Applied Sciences,
University of Tsukuba,
Tsukuba, Ibaraki 305-8573, Japan
e-mail: msislam29@yahoo.com

Q. R. Yin
Shanghai Institute of Ceramics, CAS,
Shanghai 200050, China

A- site cation by a small size ion [16]. In this contrast, MnO_2 can be a typical additive due to the multi-valance nature of Mn ions; such as Mn^{2+}, Mn^{3+}, and Mn^{4+}, which may be very effective to regulate electrical properties. On the other hand, the ionic radius of Ce^{4+} ion is close to that of Ca^{2+} ion but effective charge is different, which could be effective to regulate the oxygen vacancy and improve electrical performance [17]. By considering these phenomena, MnO_2 and CeO_2 have been chosen as the doping element to improve the ferroelectric and the dielectric properties. Although, a ferroelectric to paraelectric phase transition of CSBT is reported at 667°C [14], the phase transition dynamics is yet to be clarified.

In this study, we have investigated the CeO_2 and MnO_2 doping effect on the phase transition and the dielectric properties of CSBT using an X-ray diffraction (XRD), a scanning electron microscopy (SEM), dielectric, and Raman scattering measurements.

2 Experimental

CeO_2 and MnO_2 (0.1 wt.%) doped CSBT ceramics (abbreviated as CSBT-Ce and CSBT-Mn, respectively) were prepared by a conventional solid state reaction method at Shanghai Institute of Ceramics, Chinese Academy of Sciences [18]. The high purity raw materials, Bi_2O_3, $CaCO_3$, $SrCO_3$, TiO_2, CeO_2 and MnO_2 powdered were mixed according to a stoichiometric ratio with the nominal compositions, followed by ball milling for 24 h, and then dried and calcined at 800–900°C for 2 h. The calcined mixture was crushed by ball milling for 24 h, and then mixed with 5 wt. % polyvinyl alcohol (PVA) binder for pressing into disks of 12 mm in diameter and 2 mm thickness. The disk samples were finally sintered at 1100 to 1220°C for 30 min in air. The relative density of the sintered samples was about 96–97% of the theoretical value.

The phase purity and the crystal structure were examined by X-ray diffractometer (Panalytical, Philips) with Cu K alpha radiation. The micro-structural investigation was conducted by SEM (JSM-5610, JEOL). For SEM study all the samples were coated with gold film (15 nm) by sputtering. Then the coated samples were placed in the vacuum chamber and SEM measurements were performed with 20 kV operating voltage and 21 mm distance. The dielectric properties were measured by using an impedance/gain phase analyzer (SI1260, Solartron) with heating and cooling rate 1°C/min up to 860°C using a compact furnace with PID controller. The light source used for Raman scattering was a diode-pumped solid-state laser (Torus, Laser Quantum) with a wavelength of 532 nm and a power of approximately 50 mW. The right angle scattering was measured with a triple-grating spectrometer (T64000, Jovin-Yvon). The spectral resolution was 2 cm^{-1} for all measurements. The Raman signals were detected using a photomultiplier (R464S, Hamamatsu Photonics). For the temperature dependence of Raman scattering, a heating and cooling stage (THMS600, Linkam) was used to change the temperature of a sample in the range from 20 to 600°C. The temperature stability is within ±1°C.

3 Results and discussion

3.1 XRD and SEM

The XRD patterns of the three samples are shown in Fig. 1, where the diffraction peaks are indexed referring to JCPDS Card no. 43-0973($SrBi_4Ti_4O_{15}$). All samples are in a single phase and no secondary phase is detectable. The micrographs of SEM are shown in Fig. 2, a uniform, identical, and plate like grain morphologies are observed for all samples. The impurity free and a single phase diffraction pattern with the identical grain morphology demonstrate that both the Ce and the Mn ions are homogeneously dissolved in the pseudo-perovskite crystal lattice. The site occupancy is discussed in the following section by considering the ionic radius and the analysis of dielectric and Raman data.

3.2 Dielectric properties

Figure 3 shows the temperature dependences of dielectric constants of CSBT, CSBT-Ce, and CSBT-Mn measured at 500 kHz, and sharp dielectric anomalies are observed around 672, 668 and 687°C, respectively, corresponding to an orthorhombic to tetragonal phase transition. The observed T_C of CSBT is in good agreement with the results reported in literature [11, 12, 14]. It is found that T_C remains constant with the MnO_2 doping, while it goes to a 15°C

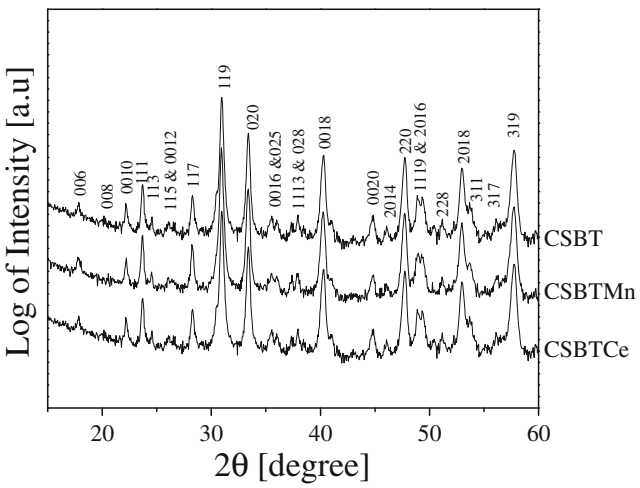

Fig. 1 XRD patterns of CSBT, CSBT-Mn and CSBT-Ce ceramics

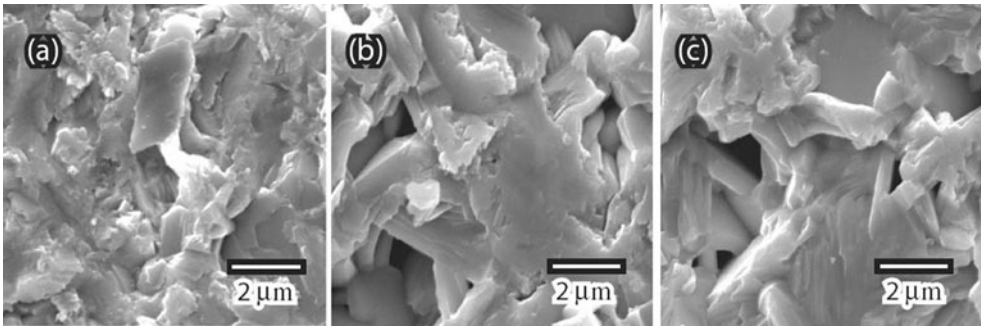

Fig. 2 SEM micrographs of (**a**) CSBT, (**b**) CSBT-Mn, and (**c**) CSBT-Ce ceramics

higher due to the CeO_2 doping. It has been reported that Mn-ion exists as Mn^{3+} ion and occupies both of the A and B-sites in a perovskite unit. As a result, there is no noticeable structural change and the T_C does not alter significantly [18]. In contrast, the variation of T_C due to the CeO_2-doping can be explained by considering the ionic radius of the constituent atoms. The ionic radius of Ce^{4+} (0.97 Å) ion is close to the A-site Ca^{2+} (1.12 Å) and Bi^{3+} (1.17 Å) ions [19]. Therefore, Ce^{4+} may replace A-site ions Bi^{3+} and/or Ca^{2+} ion. It is due to the small ionic radius of Ce^{4+} ion that augmented the distortion of TiO_6, and T_C accelerates from 672 to 687°C [20].

The dielectric maximum (ε_m) of CSBT-Ce and CSBT-Mn varied markedly due to the doping and it goes to the minimum for CSBT-Mn. These decreases of dielectric maxima can be explained in account of the polarizability. The dielectric response depends on the four kinds of polarization: electronic, ionic, dipolar and space charge polarization [17]. The effectiveness of each components have a characteristic frequency range i.e. electronic, ionic, dipolar and space charge polarization follows the optical, infrared, microwave and kilohertz or even lower frequency ranges, respectively [21]. As the measured frequency is 500 kHz, therefore, the observed lowering of dielectric response is related to the space charge polarization. The more specifically one can conclude that the number of defects are reduced due to the ions doping, consequently, degree of space charge polarization become reduced.

For a normal ferroelectric material, which undergoes a displacive phase transition, the dielectric constant ϵ (T) obeys the well known Curie-Weiss law [22]

$$\varepsilon = C/(T - T_0),\ T > T_C, \tag{1}$$

$$\varepsilon = C'/(T - T_1),\ T < T_C, \tag{2}$$

where C and C' are the Curie constants and T_0 and T_1 are the extrapolated temperatures above and bellow T_C, respectively and its follow the following relations near T_C;

$$2^{nd}\text{order}: T_0 = T_C = T_1 \text{ and } C' = C \quad \text{above } T_C, \tag{3}$$

$$1^{st}\text{order}: T_0 < T_C < T_1 \text{ and } C' = 8 \text{ just below } T_C, \tag{4}$$

Therefore, the order of ferroelectric to paraelectric phase transition can be determined from the temperature dependent inverse plot of dielectric constant ($1/\epsilon$). The reciprocal of dielectric constant vs temperature plot is shown in inset of Fig. 3(a). The obtained extrapolated temperature $T_0 < T_C$ and $T_1 > T_C$ satisfy the condition of a first order phase transition, while the Curie constant does not satisfy properly. However, a thermal hysteresis is clearly observed for all compositions (not shown) that supports the first order nature of a phase transition.

Figure 3(b) also shows the temperature dependence of dielectric loss (tanδ). At room temperature, it is very low for

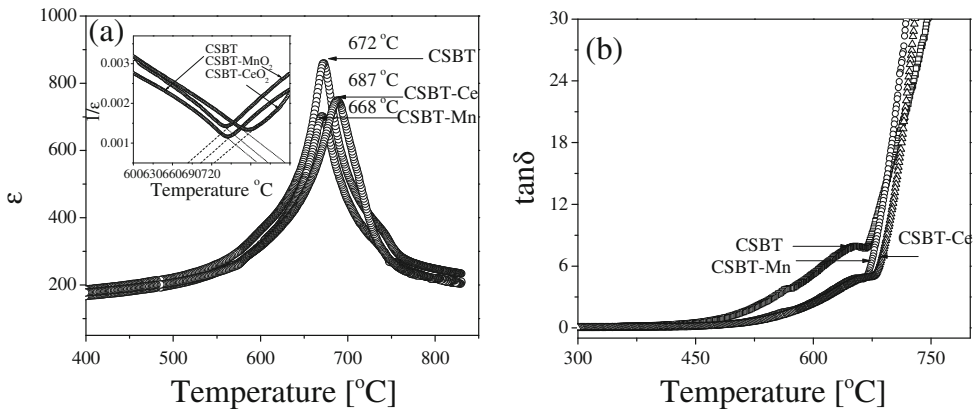

Fig. 3 (**a**) Temperature dependence of dielectric constants (inset: inverse plot of dielectric constant) and (**b**) Temperature dependence of dielectric loss of CSBT, CSBT-Mn, and CSBT-Ce ceramics

all compositions and remains constant up to 450°C and then increases drastically. This could be caused by a higher concentration of conduction carrier (positive and negative vacancies) especially at the higher temperature [20]. As, the samples were sintered at high temperature, therefore, the oxygen vacancy ($V_O^{\bullet\bullet}$) is a common defect in the studied ceramics and the influences of $V_O^{\bullet\bullet}$ become prominent at high temperature region (300–700°C) [20]. Due to the A-site replacement of $Bi^{3+}$and or Ca^{2+} ion by Ce^{4+} ion may produce bismuth/or calcium vacancy, $Ce_{Bi}^{'}$/or $Ce_{Ca}^{''}$. These cation vacancies combined with $V_O^{\bullet\bullet}$ produce $[Ce_{Bi}^{'}V_O^{\bullet\bullet}]$/or $[Ce_{Ca}^{''}V_O^{\bullet\bullet}]$ types of defect dipole. In contrast, due to the B-site replacement of Mn^{3+} produce titanium vacancy $Mn_{Ti}^{'}$ that also combined with $V_O^{\bullet\bullet}$ produce $[Mn_{Ti}^{'}V_O^{\bullet\bullet}]$ types of defect dipole. As a result, the tanδ decreases significantly due to the doping comprising with pure CSBT. The detail of defect chemistry can be found elsewhere [17, 23, 24].

The AC conductivity can be defined as $\sigma=\omega\varepsilon_0\varepsilon\tan\delta$, where ω, ε_0, ε, and tanδ are the angular frequency, permittivity of free space, relative permittivity, and loss tangent, respectively. Figure 4 shows the Arrhenius plot of σ within the temperature range 440∼640°C and the calculated activation energy. It can be seen that the conductivity decreases considerably owing to the element doping especially at the high temperature region. At the low temperature region, the conductivity is presumably predominated by the extrinsic defects, while at the high temperature region ~300–~700°C conduction is predominated by the intrinsic defects [20]. It is known that in a single phase materials with homogeneous microstructure the conductivity depends on both the mobility and concentration of the charge carries and the conductivity can be presented by the following empirical equations [10, 17]:

$$\sigma = nq\mu = \sigma_0 \exp(-E_a/k_BT) \quad (5)$$

where σ_0 is a pre-exponential factors and a characteristic of materials, n, q, μ, E_a, k_B and T is the concentration of charge carrier, number of charge per carrier, ionic mobility, activation energy for conduction, Boltzmann's constant, and absolute temperature, respectively. The improvement of conductivity can be explained by considering the bond

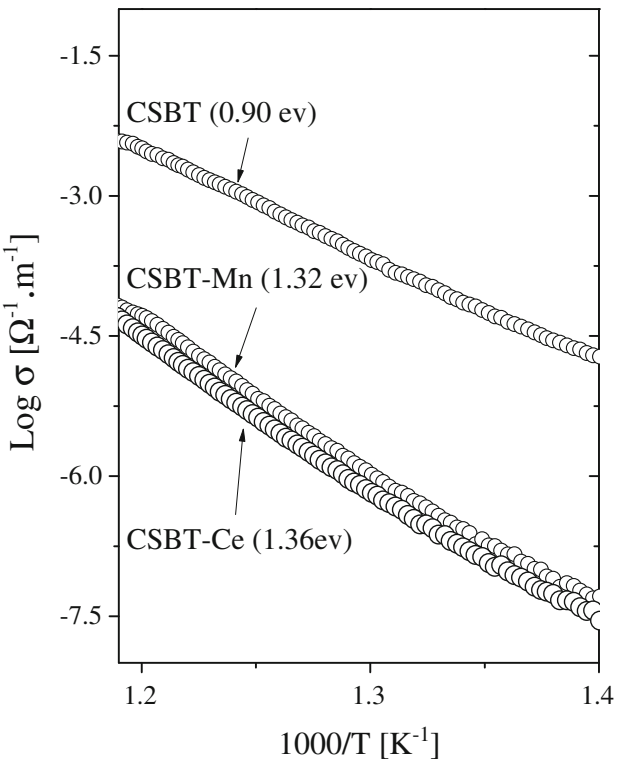

Fig. 4 AC conductivity of CSBT, CSBT-Mn, and CSBT-Ce ceramics, as a function of temperature

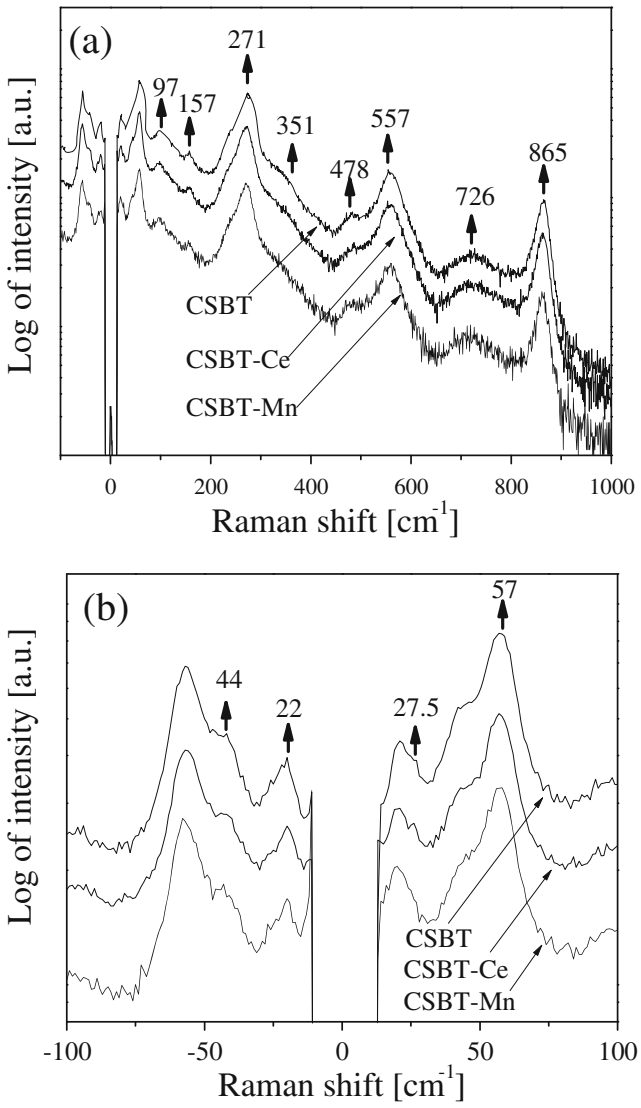

Fig. 5 Room temperature Raman spectra of CSBT, CSBT-Mn, and CSBT-Ce ceramics in (**a**) the full range spectrum, and (**b**) the low frequency region

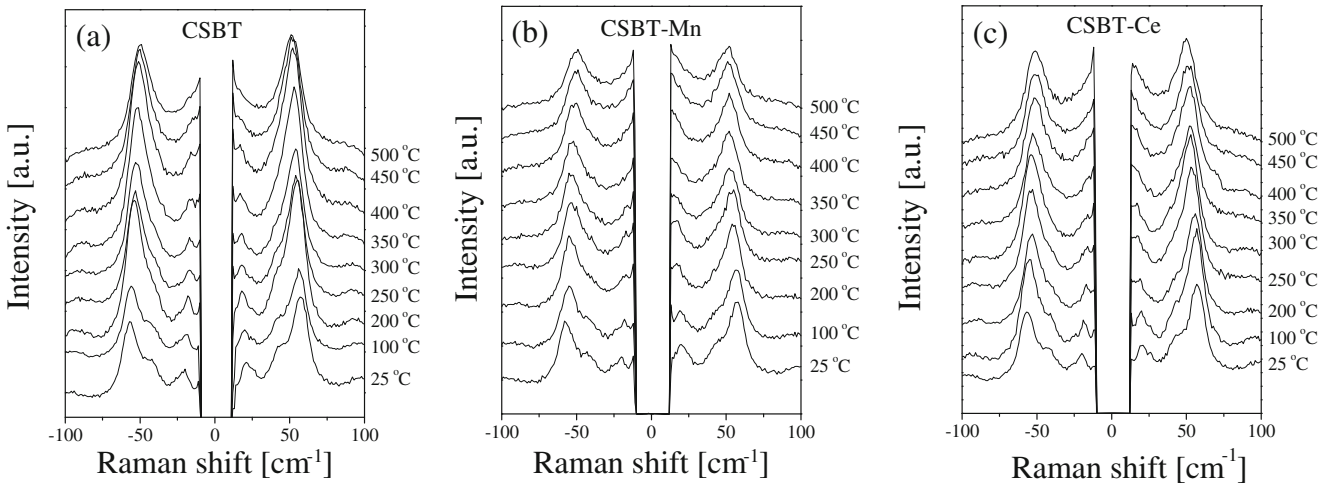

Fig. 6 Temperature dependence of Raman spectra of (**a**) CSBT, (**b**) CSBT-Mn, and (**c**) CSBT-Ce ceramics, in the low frequency region

energy. The bond energy of Mn-O in Mn_3O_4 is 1386 kJ/mol, which is higher than the Ti-O (667*kJ/mol)* [15, 25]. On the other hand, the bond energy of Ca-O and Sr-O and Ce-O are 383.3±5, 426.3±7, and 790*kJ/mol*, respectively [25]. The substitution of Ce^{4+}, Mn^{3+} and Mn^{3+} ions in the A and B-sites cations enhanced the stability of the perovskite lattice due to the increase of bond strength. The higher bond energy will effectively suppress the intrinsic defect formation. As a result, at elevated temperature, the electrical conductivity reduced significantly. The E_a of the CSBT, CSBT-Mn and CSBT-Ce are 0.90, 1.32 and 1.36 eV, respectively, calculated by using Eq. 3. This incrimination of activation energy is coherently related with the bond energy.

3.3 Raman scattering

Figure 5 shows the Raman spectra of the studied ceramics observed at room temperature. The Raman spectra exhibit intense phonon modes at 22, 57, 97, 157, 271, 478, 557, 726, and 865 cm^{-1} as well as some weak peaks. The phonon modes can be classified into two groups i.e. the internal modes of TiO_6 octahedron located >200 cm^{-1} and the lattice modes involved in the motion of the cations located <200 cm^{-1}. The detailed of the mode identification was reported in literature [10, 26, 27]. The line shapes of spectra are almost invariant at room temperature, while the scattering intensity decreases drastically due to the CeO_2 and MnO_2 doping. It is well known that spectral intensity is related to the imaginary part of the dynamic susceptibility as well as the transmission property of the sample surface. The color of the studied sample become darkens due to the CeO_2 and MnO_2 doping [28]. Therefore, the observed reduction of scattering intensity may be caused by the sample color.

The low frequency Raman spectra at room temperature are shown in Fig. 5(b). Two sharp peaks are observed at 22 and 57 cm^{-1} as well as two shoulders appeared at 27.5 and 44 cm^{-1}. In BLSFs with m=3 and 4, three soft modes are predicted: the relative a-axis displacement of Bi ions in the ferroelectric phase in the pseudo-perovskite layer with respect to the chain of a TiO_6 octahedron at 22 cm^{-1}; the rotational mode of the TiO_6 octahedron along the a-axis at

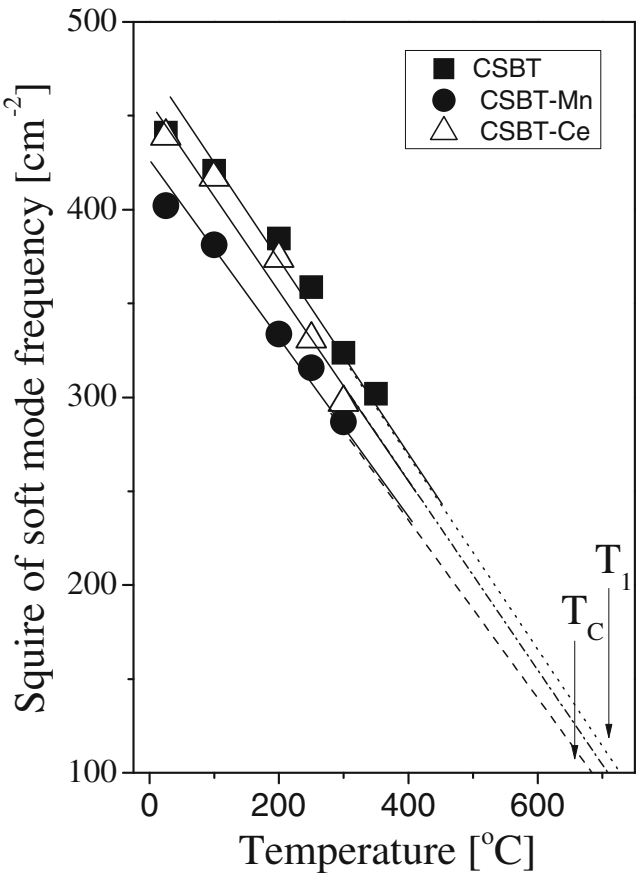

Fig. 7 The square of soft mode peak frequency of CSBT, CSBT-Mn, and CSBT-Ce ceramics, as a function of temperature

27.5 cm^{-1}; and another rotational mode of the TiO_6 octahedron along the *c*-axis at 44 cm^{-1} [9, 26, 27, 29]. The mode frequency at 22 and 44 cm^{-1} slightly decreases, while the frequency of the rigid layer mode at 57 cm^{-1} unchanged in CBT-Ce and CSBT-Mn. This fact indicates the occupation of A-site in the pseudo-perovskite layer by Ce^{4+} and Mn^{2+} ions.

To get new insights into the dynamics of the phase transition, the temperature dependence of soft optical phonon was investigated as shown in Fig. 6. With the increase of temperature the phonon modes at 27.5 and 44 cm^{-1} become weak and broad, and finally disappear above 350° C. The rigid layer mode at 57 cm^{-1} originated from the vibration of rigid Bi_2O_2 layer also shifts toward the lower frequency, but still observed clearly up to 600°C. With the increase of temperature, the mode frequency at 22 cm^{-1} shows a significant softening and finally overdamped around 500°C. Therefore, this mode can be a soft phonon mode, which is responsible to the structural phase transition. Figure 7 shows the temperature dependence of square of the soft mode peak frequency (ω_s^2), and it monotonically decreases towards the T_1, the extrapolated temperature at which ω_s^2 goes to zero. The fact $T_1 > T_C$ is a common feature of a first order phase transition [10, 25]. While the damping of soft mode randomly increase with the increase of temperature that can be explained by considering the local strain in the pseudo-perovskite unit. The observed ratio approximately$C : C^{'} = 1 : 1$and the difference between T_1 and T_C, is rather small for all compositions. As there are some differences of ionic radii among the host (Ca, Sr, and Bi) and doping (Ce and Mn) ions that may induce some internal strain in the pseudo-perovskite unit. Such a local strain may couple with the soft optic mode. This coupling could be responsible for this dielectric anomalous behavior of *C*: *C′* ratios and the increase of damping of soft mode.

4 Conclusions

The CeO_2 and MnO_2 doping effect on the dynamical physical properties of CSBT ceramics were investigated by using XRD, SEM, temperature dependent dielectric and Raman scattering measurements. The numerical values of dielectric constant were found as 850±10 (CSBT), 740±10 (CSBT-Ce), and 690±10 (CSBT-Mn) and the T_C of CSBT-Ce was enhanced from 672 (CSBT) to 687°C due to the crystal lattice distortion. The dielectric losses were reduced from 8 to 5 and the AC conductivity was decreased 2 times with in the temperature region ~500~700°C, due to the reduction of conducting carriers through defect dipole formation. The thermal hysteresis of a dielectric susceptibility and the fact that square of soft mode frequency ω_s^2 was approximately proportional to T_1-T ($T_C < T_1$) indicated the first order nature of a ferroelectric phase transition. The *C*: *C′* ratio was 1:1 and the scattered nature of damping constant of the soft optic mode demonstrated a coupling of soft mode with the local strain induced by doping. This coupling may enhance the piezoelectric performance of doped-CSBT.

References

1. S. Ikegami, I. Ueda, Jpn. J. Appl. Phys. **13**, 1572 (1974)
2. B.H. Park, B.S. Kang, S.D. Bu, T.W. Noh, J. Lee, W. Jo, Nature **401**, 682 (1999)
3. A. Ando, M. Kimura, Y. Sakabe, Jpn. J. Appl. Phys. **42**, 2009 (2003)
4. M.S. Islam, S. Tsukada, S. Kojima, M.-S. Jang, J. Korean Phys. Soc. **55**(2), 908 (2009)
5. B. Aurivillius, Arkiv Kemi **1**, 499 (1949)
6. B. Aurivillius, Arkiv Kemi **2**, 519 (1950)
7. E.C. Subbarao, J. Phys. Chem. Solids **23**, 665 (1962)
8. E.C. Subbarao, J. Am. Ceram. Soc. **45**, 166 (1962)
9. S. Kojima, J. Phys. Condens. Matter **10**, L327 (1998)
10. M.S. Islam, J. Kano, S. Tsukada, Q. Yin, S. Kojima, Jpn. J. Appl. Phys **48**, 09KC101 (2009)
11. L. Zheng, G. Li, W. Zhang, Q. Yin, Jpn. J. Appl. Phys. **41**, L1471 (2002)
12. H. Yan, C. Li, J. Zhou, L. He, W. Zhu, Y. Song, Y. Yu, Jpn. J. Appl. Phys. **40**, 6501 (2001)
13. L.-X. He, C.-E. Li, J. Mater. Sci. **35**, 2477 (2000)
14. Z. Liaoying, L. Guorong, Z. Wangzhong, C. Daren, Y. Qinrui, Mater. Sci. Eng. B **99**, 363 (2003)
15. E.C. Subbarao, Phys. Rev. **122**, 804–807 (1961)
16. M.J. Forbess, S. Seraji, Y. Wu, C.P. Nguyen, G. Cao, App. Phys. Lett. **76**, 2934 (2000)
17. C.-M. Wang, Wang J-F, S. Zhang, T.R. Shrout, J. Appl. Phys. **105**, 0941101 (2009)
18. G. Li, L. Zheng, Q. Yin, B. Jiang, W. Cao, J. Appl. Phys. **98**, 064108-1 (2005)
19. R.D. Shannon, Acta Crystallogr. A **32**, 751 (1976)
20. Y. Wu, M.J. Forbess, S. Seraji, S.J. Limmer, T.P. Chou, C. Nguyen, G. Cao, J. App. Phys. **90**, 5296 (2001)
21. R.E. Newnham, *Properties of Materialas: Anisotropy, Symmetry, Structure* (Oxford Uvi. Press, 2005)
22. F.M. Pontes, L.S. Santos, D.S.L. Pontes, E. Longo, S.C. Neto, E.R. Leite, A.J. Chiquito, P.S. Pizani, J. Appl. Phys. **104**, 014107–1 (2008)
23. R. Merkle, J. Maier, Phys. Chem. Chem. Phys. **5**, 2297 (2002)
24. J. Jeong, Y.H. Han, Phys. Chem. Chem. Phys. **5**, 2264 (2003)
25. R.C. Weast, M.J. Astle, W.H. Beyer, *CRT Hand Book of Chemistry and Physics*, 89th edn. (CRC, FL, 2008)
26. S. Kojima, S. Shimada, Physica B **219 & 220**, 617 (1996)
27. A. Hushur, J.-H. Ko, S. Kojima, S.S. Lee, M.-S. Jang, J. Korean Phys. Soc. **41**, 763 (2002)
28. W. Hayes, R. Loudon, *Scattering of Light by Crystals* (Dover, N. Y., 2004)
29. A.D. Rae, J.G. Thompson, R.L. Withers, A.C. Willis, Acta Crystrallogr. B **46**, 474 (1990)